

International Conference on Space Optics—ICSO 2006

Noordwijk, Netherlands

27–30 June 2006

Edited by Errico Armandillo, Josiane Costeraste, and Nikos Karafolas



EOS-AURA ozone monitoring instrument: scientific results of nearly two years successful operation and in-flight calibration and performance

M. Dobber, R. Dirksen, P. Levelt, B. van den Oord, et al.



EOS-AURA OZONE MONITORING INSTRUMENT: SCIENTIFIC RESULTS OF NEARLY TWO YEARS SUCCESSFUL OPERATION AND IN-FLIGHT CALIBRATION AND PERFORMANCE

M. Dobber⁽¹⁾, R. Dirksen^(1,2), P. Levelt⁽¹⁾, B. van den Oord⁽¹⁾, R. Voors⁽¹⁾, Q. Kleipool⁽¹⁾

⁽¹⁾Royal Netherlands Meteorological Institute, PO Box 201, 3730 AE De Bilt, NL, dobber@knmi.nl;

⁽²⁾Space Research Organisation Netherlands, Sorbonnelaan 2, 3584 CA Utrecht, NL

ABSTRACT

The OMI instrument is an ultraviolet-visible imaging spectrograph that uses two-dimensional CCD detectors to register both the spectrum and the swath perpendicular to the flight direction with a 115° wide swath, which enables global daily ground coverage with high spatial resolution. This paper presents a number of examples of scientific results from the first two years in orbit, as well as a selection of in-flight radiometric, spectral and CCD detector performance and calibration results. The scientific results will show the OMI capability of measuring atmospheric phenomena with high spatial and temporal resolution. It will be shown that the OMI radiometric and spectral calibration are accurately understood. Radiation damage effects on the CCD detectors will be discussed in detail and it will be shown that it is possible to correct for the consequences to a large extent in order to minimise the impact on the scientific level-1 and level-2 data products.

1. INTRODUCTION

The Ozone Monitoring Instrument (OMI) was launched on 15 July 2004 on NASA's EOS AURA satellite. The primary objective of the OMI instrument is to obtain daily global measurements of ozone and nitrogen dioxide in both the troposphere and stratosphere. The central science issues addressed by the OMI mission are the recovery of the ozone layer, the depletion of ozone at the poles, tropospheric pollution and climate change. In addition, OMI is intended as the successor to the Total Ozone Mapping Spectrometer (TOMS) operated by NASA over the past 25 years [1-4].

OMI combines a high spatial resolution and daily global coverage. In this way tropospheric trace gases can be observed with high spatial resolution and cloud-free ground pixels are more easily obtained as compared to instruments with scanning mirrors. OMI will deliver absolutely calibrated spectral radiances and irradiances in the spectral range from 264-504 nm. These are used to retrieve the primary data products: ozone total column, ozone vertical profile, UV-B flux,

nitrogen dioxide total column, aerosol optical thickness, cloud effective cover, cloud top pressure and secondary data products: total column SO₂, BrO, HCHO and OCIO. The atmospheric constituent concentrations are retrieved from nadir observations of backscattered light from the sun on the earth's atmosphere in the ultraviolet-visible wavelength range (264-504 nm) using both Differential Optical Absorption Spectroscopy (DOAS) algorithms and algorithms that have been used before in the TOMS instrument series. The ozone profile is obtained from strong wavelength dependence of the absorption cross-section between 270 and 330 nm.

OMI follows in the footsteps of predecessor instruments like the Global Ozone Monitoring Instrument (GOME) on ERS-2, the Scanning Imaging Absorption Spectrometer for Atmospheric Cartography (SCIAMACHY) on ENVISAT, TOMS and Solar Backscatter UltraViolet (SBUV), but OMI features a number of important improvements over these earlier generation instrument. By combining a unique telescope design with the use of two-dimensional frame transfer CCD detectors a 115 degrees large field-of-view perpendicular to the flight direction can be covered. This yields a 2600 km wide ground swath that is wide enough to achieve daily global coverage of the earth's atmosphere at the equator at a resolution of 13x24 km² (flight direction x swath direction) in the nadir direction. By employing a two-dimensional CCD the spectrum of every ground pixel is recorded simultaneously. In one CCD dimension the spectrum is recorded, while the viewing direction is recorded in the other dimension. The operational temperature of the optical bench is 264 K and the temperature of the CCD detectors is stabilised at a temperature of 265 K. The telescope also contains a polarisation scrambler, that ensures that the instrument is insensitive to the polarisation state of the incident light. This increases the radiometric accuracy of the earth and sun measurements. For the sun observation mode OMI is equipped with a quartz volume reflectance diffuser that has been optimised to introduce minimal wavelength and viewing direction dependent structures in the measured signals. Further

details on the OMI design and calibration are given in [1].

For remote sensing instruments like OMI a good on-ground calibration delivering reliable calibration key data for 0-1 data processing ,as well as an extensive and continuous in-flight calibration, are essential to meet the required accuracies for the target scientific data products, especially when the data is to be compared to and to become part of long-term ozone trend records.

OMI has been developed by Dutch and Finnish industry in close collaboration with the climate research and meteorological community and under contract with the Netherlands Agency for Aerospace Programmes (NIVR) and the Finnish Meteorological Institute (FMI). The Royal Netherlands Meteorological Institute (KNMI) is the Principal Investigator (PI) institute for the OMI instrument.

This paper describes and discusses a number of representative results from the first two years of OMI in orbit, as well as a number of in-flight radiometric and detector calibration results. An accompanying paper with more details on the OMI in-flight calibration and performance can be found in [7].

2. OMI RESULTS

As described in the introduction, a distinct advantage of the OMI measurement data is that the state of the atmosphere of the earth can be measured with daily global coverage and high spatial resolution. This enables to investigate atmospheric pollution phenomena on urban scales. Fig. 1 shows an example of the tropospheric NO₂ column in de Randstad, The Netherlands. The spatial extent of the red spot is about 50 km x 50 km. Such pollution phenomena are highly variable in place and time and depend strongly on the meteorological conditions at the time (temperature, wind, precipitation). This means that the atmospheric situation for the previous or the next day can be completely different. The time evolution of a parameter such as the tropospheric NO₂ column can be monitored with OMI with a time resolution of one day or even higher, depending on the latitude of the observed spot on earth. In order to measure tropospheric atmosphere constituents accurately the observed ground pixels shall be free of clouds. With its high spatial resolution of 13x24 km² OMI has a comparatively high probability of looking in between clouds if clouds are present. Fig. 2 shows a similar example of the Nantes / Orleans / Saint-Etienne area in France. It can be seen that the individual larger and smaller cities can easily be identified. Figs. 1 and 2 are actually regridded examples on a 0.02° x 0.02° grid. In order to make these pictures on such a high density grid the OMI measurement data from one year have been used.

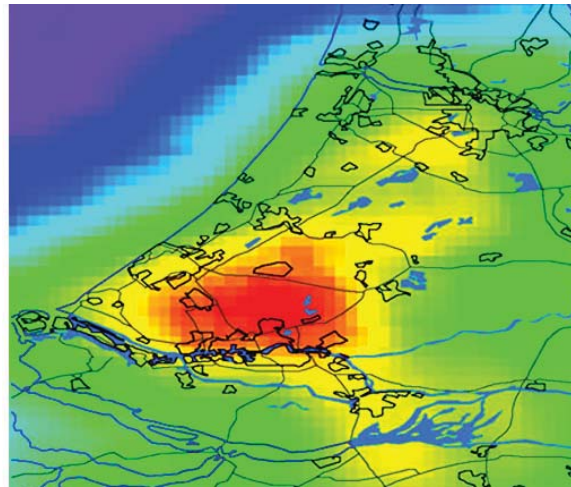


Fig. 1. Example of tropospheric NO₂ column in de Randstad, The Netherlands (regridded, courtesy P. Veeffkind, KNMI).

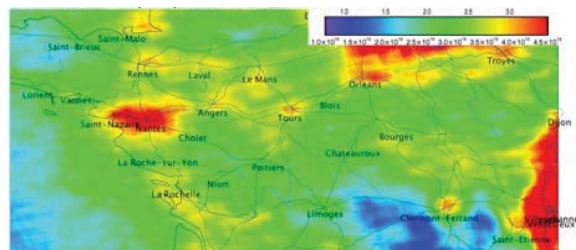


Fig. 2. Example of tropospheric NO₂ column in the Nantes / Orleans / Saint-Etienne area in France (regridded, courtesy P. Veeffkind, KNMI).

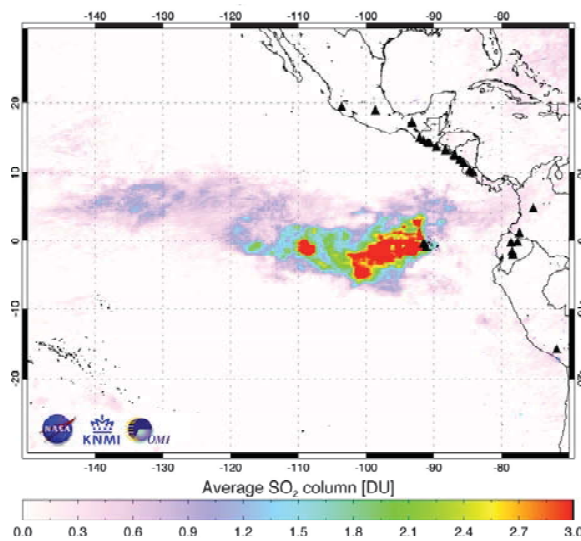


Fig. 3. Average SO₂ column for an eruption of the Sierra Negra volcano on the Galapagos Islands (courtesy Simon Carn, UMBC, Baltimore, MD).

Fig. 3 shows an example of SO₂ as measured by an eruption of the Sierra Negra volcano on the Galapagos Islands. SO₂ produces a weak absorption signal in the

measured images in a spectral band around 310 nm, where ozone produces strong absorption features as well. Fig. 3 thus demonstrates both the high spatial resolution with which such events can be measured by OMI and the sensitivity of the OMI instrument to measure weakly absorbing atmospheric constituents. In addition, the time evolution of the volcanic eruption can be followed on a daily time resolution.

3. RADIOMETRIC CALIBRATION

During the on-ground calibration of the OMI instrument the spectral slit functions as a function of wavelength and viewing direction have been calibrated accurately using a method and experimental measurement setup especially designed for OMI [5-7]. Using these accurately calibrated spectral slit functions it is possible to convolve a literature high-resolution solar spectrum to OMI spectral resolution and compare the result with the irradiance as measured by OMI in flight over the quartz volume diffuser. The result of this analysis is shown in Fig. 4.

Any deviations from unity may be caused by:

- Errors in the OMI radiometric irradiance calibration.
- Errors in the OMI wavelength calibration.
- Errors in the determined OMI spectral slit functions.
- Errors in the high-resolution solar reference spectrum.

These four possibilities were carefully investigated and changes were made to all of the above parameters. Fig. 4. shows that the calibration of the OMI irradiance is well understood within the expected accuracies. In the same analysis an accurate high-resolution solar reference spectrum was obtained.

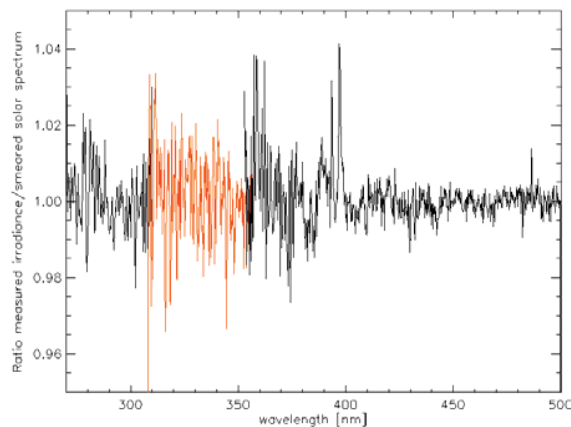


Fig. 4. Ratio of measured irradiance from orbit 2465 (31 December 2004) over high-resolution solar reference spectrum convolved with OMI spectral slit functions.

4. SPECTRAL CALIBRATION

The in-flight wavelength calibration for OMI is performed by use of the Fraunhofer lines in the sun and earth spectra. The results of the in-flight wavelength calibration on earth spectra along complete orbits show wavelength shifts of up to 0.5 pixel when the signal intensity changes, i.e. when the ground scene changes in the flight direction, e.g. in case of clouds. This holds particularly for the UV2 and VIS channels, but not for the UV1 channel, because for wavelengths below 305 nm the ground is not seen and scene-to-scene variability is much less. The effect can be explained in terms of partial or non-uniform filling of the spectrometer's entrance slit in the flight direction, which is also the spectral dispersion direction. It turns out that it is possible to correct accurately for this effect, that is the main error source in the spectral calibration, by using the so-called small-pixel column data in the UV2 and VIS channel. Small pixel data, one column in the UV2 channel and one in the VIS channel, are available at a higher read-out frequency than the regular images. The correction for the observed wavelength shift makes use of the correlation that exists between the observed wavelength shifts and the gradients in the small-pixel column data. Fig. 5 shows an example of this correlation in the VIS channel for an arbitrary orbit. By applying the wavelength correction for changing scenes in the 0-1 data processing the accuracy of the in-flight wavelength calibration of earth shine spectra is improved to about 0.02 px in UV1 and 0.01 px in UV2 and VIS, which is the goal accuracy for the in-flight wavelength calibration. More details about the correction to the spectral calibration for inhomogeneous ground scenes can be found in [8].

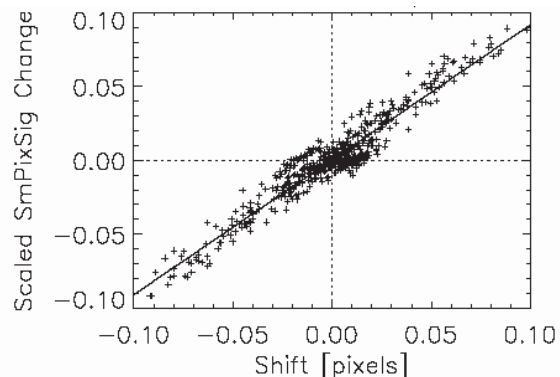


Fig. 5. Correlation for earth shine spectra between wavelength shifts close to cloud transitions and gradients in small pixel column readouts for the VIS channel. This effect is attributed to partial slit illumination at inhomogeneous ground scenes and is corrected in the 0-1 data processor using a correlation as shown. In the figure the correlation coefficient is 0.96, the slope is 0.92.

5. DETECTOR DARK SIGNALS

It is well known from the literature that protons from the space environment can cause damage to the CCD detectors [9-12]. In this section the CCD detector performance during the first 1.5 years in orbit is investigated. Once per day the CCD detectors are read out in unbinned mode on the eclipse side of the orbit with the folding mirror blocking the optical light path. These measurements are particularly well suited to determine dark currents of the individual (unbinned) pixels. Fig. 6 shows a representative example from 24 October 2004 (red curve). The average dark signal is about 1700 BU, but hot pixels with higher signals can be clearly identified. A similar picture at the beginning of the mission or pre-flight shows no such hot pixels (red curve in Fig. 6). The peaks of the individual pixels originate from an increase in dark signal or dark current after the pixel was hit by a damaging particle, most likely a proton. For OMI we found that the increase in dark current can be up to a factor 10 for unbinned pixels. It must be noted that the peaks as shown in Fig. 6 can not be attributed to single events, such as the ones observed when the instrument passes through the South Atlantic Anomaly (SAA). In such cases increased activity is observed on the CCD images, but the increased signals disappear once the spacecraft leaves the SAA. An example of such increased temporary activity SAA behaviour is shown in Fig. 7. In contrast, the peaks as shown in Fig. 6 represent a permanent increase in dark current resulting from permanent damage to the CCD pixel in the form of lattice displacements. It must also be noted that Fig. 6 represents a measurement with an exposure time of 136 seconds and a gain factor of 40. For the usual exposure times of 0.5-2.0 seconds and gain factors of 1-10 used for earth and sun measurements the increase in dark signal is much less.

Fig. 8 shows the number of hot pixels as a function of time after launch for the image areas of the UV and VIS CCD detectors. It can be seen that the number of hot pixels increases about linearly with time and that the line extrapolates more or less through zero at launch, as expected.

Another way to visualise the changes in the CCD detector dark signal is to investigate the CCD histograms of the dark measurements. Figs. 9 and 10 show such histograms for two measurements with exposure times of 36 seconds and gain factor 40 obtained on 20 August 2004 and 5 February 2005. It can be observed that the tail of the distribution towards higher signals increases with time. This behaviour is known from and consistent with on-ground radiation testing with protons.

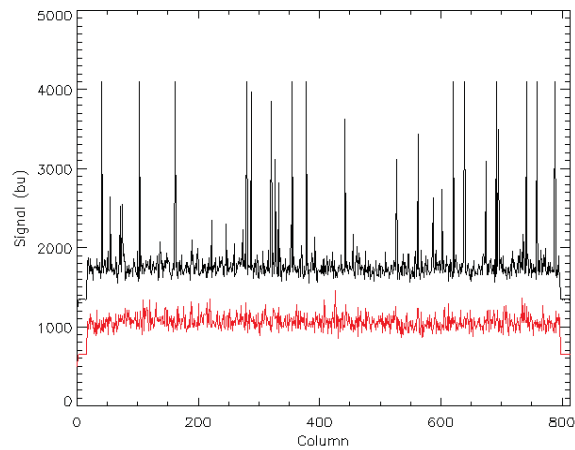


Fig. 6. Signal for row 300 of the UV channel on 24 October 2004 in the CCD image area (black curve). The red curve shows the same CCD row as measured prior to launch. The red curve of the pre-launch data has been given an offset of 700 bu for clarity. The plot clearly shows the pixels with enhanced dark signals.



Fig. 7. Dark signal measurement with exposure time 136 seconds and gain factor 40 in South Atlantic Anomaly (SAA). The increased number of random hits and trails of particles can be observed.

UV (blue) and VIS (red) (unbinned) CCD detector hot pixels

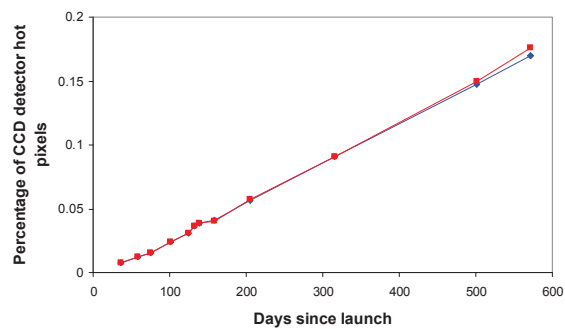


Fig. 8. Number of hot pixels as a function of time after launch for the UV (blue) and VIS (red) CCD detectors.

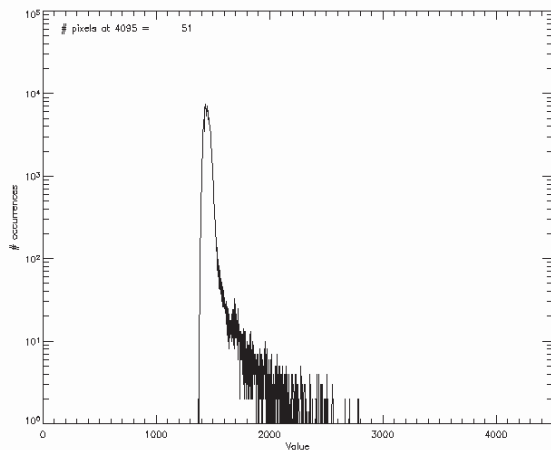


Fig. 9. Histogram of a dark signal measurement on 20 August 2004.

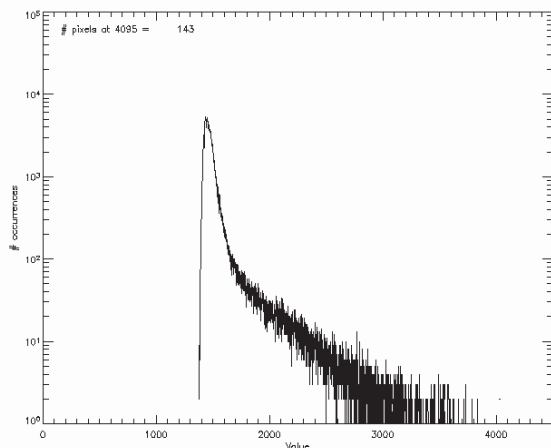


Fig. 10. Histogram of a dark signal measurement on 5 February 2005. More pixels have moved from the main peak towards the high-end tail as compared to Fig. 9.

Further investigation on the locations on the earth where hot pixels are mostly created reveals that most hot pixels with permanently increased dark current are created in the SAA and in the radiation belts of the earth. This suggests that trapped protons with high energies (>10 MeV) that are able to penetrate the 29 mm thick aluminium shield around the OMI CCD detectors are the main cause for the observed radiation damage. More studies on the origin, rate as a function of time and impact of the OMI CCD radiation damage are ongoing. In these studies other instruments with similar CCD detectors are also investigated (GOMOS on ENVISAT and OSIRIS on ODIN).

Proton radiation damage on CCD detectors is known from literature to cause a phenomenon known as Random Telegraph Signal or RTS [11, 12]. RTS in dark signal measurements manifests itself as a type of behaviour where the output of a pixel is unstable and shows evidence for jumps between multiple more or

less stable energy levels. This is a statistical process and the time constants of such jumps can vary per pixel. The exact times when an energy transition will occur can not be predicted. It is known from the literature that the time constants between jumps become longer when the CCD temperature is lowered. This behaviour has been confirmed on proton irradiated CCD samples before launch for the OMI instrument. For OMI we found that nearly all pixels that have been hit by one or more protons show RTS behaviour. However, the magnitude of the RTS behaviour can vary strongly from pixel to pixel. From inspection of the pixels with increased dark current it is estimated that about 95 percent of these pixels can still be used for useful scientific measurements, because the dark signal can be corrected for using a dynamic dark signal correction scheme. The remaining 5 percent shows damage to an extent that the pixel contents may be unreliable or inaccurate, because the dark current and/or noise shows large variations in time.

Pixels that are hit by protons thus show an increase in dark current by a factor of up to 10 and less or more serious RTS behaviour. However, such hot pixels can still be used for useful scientific measurements if earth shine spectra are corrected for dark signal with measurements that are obtained close in time to the light measurement, i.e. when the dark signal correction is sufficiently dynamic to correct for the permanent increase in dark current in a CCD pixel after a proton hit. The accuracy of such a dynamic dark signal correction scheme is influenced by the magnitude of the Random Telegraph Signal (RTS) behaviour of the pixels. In order to properly appreciate the impact of the CCD pixel proton radiation damage manifested by the increased dark current and RTS behaviour one must realise that the results shown so far have been obtained with measurements with exposure times of 136 seconds and gain factor 40. Typical earth-shine and sun measurements are performed with exposure times of 0.5-1.0 seconds and gain factors of 4 or 10, i.e. the impact of the proton damage on actual earth or sun measurements is typically three orders of magnitude smaller as discussed above. Furthermore, the earth and sun measurements are performed with electronic binning factor 4 or 8, whereas the long dark measurements shown above have been performed with binning factor 1. So even when the proton radiation damage on the CCD detectors is a compromising factor for the quality of the earth and sun measurements and the exact impact of the damage must be continuously monitored, the impact on the OMI science data is not as severe as might have been suggested by the results shown in this section, which present extreme cases obtained with extreme measurement settings that are not at all representative for the regular OMI science measurements. In order to be able to deal properly with the pixel-dependent varying dark currents of the CCD

detectors a dynamic dark signal correction scheme that is able to use the appropriate dark signal measurements close in time to the earth and sun measurements is currently in preparation.

6. CONCLUSIONS

A number of in-flight scientific, calibration and performance results of the Ozone Monitoring Instrument OMI, successfully launched on 15 July 2004 on the EOS-AURA satellite, have been presented and discussed.

Examples for tropospheric NO₂ from pollution and SO₂ from a volcanic eruption were shown. These examples show the OMI capability for measuring atmospheric phenomena with high spatial and temporal resolution.

The radiometric calibration in comparison to the high-resolution solar irradiance spectrum from the literature convolved with the measured spectral slit function was discussed.

The correction algorithm to correct for spectral shifts originating from inhomogeneous ground scenes (e.g. clouds) was presented and it was shown that the accuracy of the in-flight spectral calibration is 0.02 pixel for the UV1 channel and 0.02 pixel for the UV2 and VIS channels.

The in-flight performance of both CCD detectors shows evidence of particle hits by trapped high-energetic protons, which results in increased dark currents and increase in the Random Telegraph Signal (RTS) behaviour. The resulting detector performance changes can be to a large extent corrected for by a dynamical dark signal correction scheme, which is in preparation.

7. REFERENCES

1. M. R. Dobber, R. J. Dirksen, P. F. Levelt, G. H. J. van den Oord, R. Voors, Q. Kleipool, G. Jaross, M. Kowalewski, E. Hilsenrath, G. Leppelmeier, J. de Vries, W. Dierssen, N. Rozemeijer, Ozone Monitoring Instrument calibration, *IEEE Trans. Geosc. Rem. Sens.*, 44 (5) (2006).
2. P. F. Levelt, E. Hilsenrath, G. W. Leppelmeier, G. H. J. van den Oord, P. K. Bhartia, J. Tamminen, J. F. de Haan, J. P. Veefkind, Science objectives of the Ozone Monitoring Instrument, *IEEE Trans. Geosc. Rem. Sens.*, 44 (5) (2006).
3. P. F. Levelt, G. H. J. van den Oord, M. R. Dobber, J. Claas, H. Visser, J. de Vries, The Ozone Monitoring Instrument, *IEEE Trans. Geosc. Rem. Sens.*, 44 (5) (2006).
4. G. H. J. van den Oord, J. P. Veefkind, P. F. Levelt, M. R. Dobber, Level 0 to 1B processing and operational aspects, *IEEE Trans. Geosc. Rem. Sens.*, 44 (5) (2006).
5. R. Dirksen, M. Dobber, R. Voors, P. Levelt, Prelaunch characterization of the Ozone Monitoring Instrument transfer function in the spectral domain, *Applied Optics*, Vol. 45, no. 17, 2006.
6. M. Dobber, R. Dirksen, R. Voors, G.H. Mount, P. Levelt, Ground-based zenith sky abundances and in situ gas cross sections for ozone and nitrogen dioxide with the Earth Observing System Aura Ozone Monitoring Instrument, *Applied Optics*, Vol. 44, no. 14, 2846-2856, 2005.
7. R. Dirksen, M. Dobber, R. Voors, Q. Kleipool, G. van den Oord, P. Levelt, In-flight calibration of the Ozone Monitoring Instrument, ICSO 2006, this issue.
8. R. Voors, M. Dobber, R. Dirksen, P. Levelt, Calibration method to correct for cloud-induced wavelength shifts in Aura's Ozone Monitoring Instrument, *Applied Optics*, Vol. 45, no. 15, 2006.
9. Ch. Date et al., Displacement damage effects in mixed particle environments for shielded spacecraft CCDs, *IEEE Trans. Nucl. Sci.*, Vol. 40, no. 6, pp. 1628-1637, 1993.
10. M.S. Robbins, High energy proton-induced dark signal in silicon charge coupled devices, *IEEE Trans. Nucl. Sci.*, Vol. 47, no. 6, pp. 2473-2479, 2000.
11. I.H. Hopkins, G.R. Hopkinson, Random Telegraph Signals from proton-irradiated CCDs, *IEEE Trans. Nucl. Sci.*, Vol. 40, no. 6, pp. 1567-1574, 1993.
12. I.H. Hopkins, G.R. Hopkinson, Further measurements on Random Telegraph Signals in proton-irradiated CCDs, *IEEE Trans. Nucl. Sci.*, Vol. 42, no. 6, pp. 2074-2081, 1995.